

Hydrodynamic afterburner for the CGC at RHIC

Tetsufumi Hirano [†] and Yasushi Nara [‡]

[†]RIKEN BNL Research Center, Brookhaven National Laboratory, Upton, NY 11973, USA

[‡]Department of Physics, University of Arizona, Tucson, Arizona 85721, USA

Abstract. Firstly, we give a short review about the hydrodynamic model and its application to the elliptic flow phenomena in relativistic heavy ion collisions. Secondly, we show the first approach to construct a unified model for the description of the dynamics in relativistic heavy ion collisions.

1. A Short Review on Elliptic Flow from Hydrodynamic models

First data reported by the STAR Collaboration at RHIC [1] has a significant meaning that the observed large magnitude of elliptic flow for charged hadrons is consistent with hydrodynamic predictions [2]. This suggests that large pressure possibly in the partonic phase is built at the early stage ($\tau \sim 0.6$ fm/ c) in Au+Au collisions at $\sqrt{s_{NN}} = 130$ and 200 GeV. This situation at RHIC is in contrast to that at lower energies such as AGS or SPS where hydrodynamics always overpredicts the data [3]. Moreover, this also suggests that the effects of the viscosity in the QGP phase is remarkably small and that the QGP is almost a perfect fluid [4]. Hadronic transport models are very good to describe experimental data at lower energies, while they fail to reproduce such large values of elliptic flow parameter at RHIC (see, e.g., Ref. [5]). So the importance of hydrodynamics is rising in heavy ion physics. After the first STAR data were published [1], other groups at RHIC have also obtained the data concerning with flow phenomena [6]. To understand these experimental data, hydrodynamic analyses are also performed extensively [7, 8]. In this short review, we highlight several results on elliptic flow from hydrodynamic calculations.

1.1. Why elliptic flow?

Elliptic flow is very sensitive to the degree of secondary interactions [9]. The indicator of momentum anisotropy is the second harmonic coefficient of azimuthal distributions

[†] Present address: Department of Physics, Columbia University, New York, NY 10027, USA

[‡] Present address: Institute für Theoretische Physik, J. W. Goethe Universität, D-60054 Frankfurt, Germany

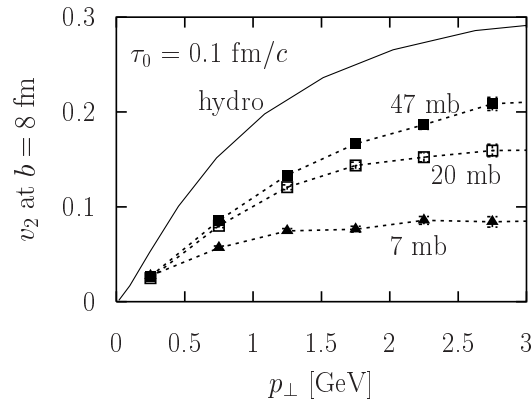


Figure 1. Comparison of the hydrodynamic result with the results obtained by a partonic transport model. Figure taken from Ref. [14].

[10]

$$v_2(p_T, y) = \frac{\int d\phi \cos(2\phi) \frac{dN}{p_T dp_T dy d\phi}}{\int d\phi \frac{dN}{p_T dp_T dy d\phi}} = \langle \cos(2\phi) \rangle. \quad (1)$$

For recent progress of higher harmonics, see Refs. [11, 12]. The spatial anisotropy

$$\varepsilon = \frac{\langle y^2 - x^2 \rangle_s}{\langle x^2 + y^2 \rangle_s}, \quad \langle \dots \rangle_s = \frac{\int \dots e(\tau, x) d^3x}{\int e(\tau, x) d^3x} \quad (2)$$

at the initial time is a seed of the momentum anisotropy. Within the hydrodynamic picture, pressure gradient along the x -axis is larger than the y -axis in non-central collisions. Here the direction of x -axis is parallel to the impact parameter vector. This is the driving force for generating v_2 . The response of the system can be defined by v_2/ε . As will be discussed later, the hydrodynamic response is almost constant $v_2/\varepsilon \sim 0.2$ -0.24 at the SPS and RHIC energies [13].

In ideal hydrodynamics, the mean free path among particles is assumed to be zero. So the hydrodynamic prediction of v_2 should be maximum among transport theories. We naively expect that the ideal hydrodynamics corresponds to the infinite limit of the cross sections among particles in collision terms of the Boltzmann equation. In Ref. [14], Molnar and Huovinen compare $v_2(p_T)$ from hydrodynamics with the one from Boltzmann equation. Special attention is paid that the same initial conditions and thermodynamic properties are used in comparison. Figure 1 shows the transverse momentum dependence of v_2 for a hydrodynamic model and a parton cascade model. $v_2(p_T)$ from Boltzmann simulations is approaching to the hydrodynamic result with increasing the cross section among partons. However, even for large cross section (47 mb), the result from the Boltzmann simulation is still $\sim 30\%$ smaller than the hydrodynamic result. This clearly shows the ideal hydrodynamics describes the strongly interacting matter.

1.2. Basics of Ideal Hydrodynamics

Here we concentrate our discussions on the ideal hydrodynamic model. For those who have interest in the viscous hydrodynamics, see, e.g., Ref. [15].

Hydrodynamic equations are nothing but the energy-momentum conservations $\partial_\mu T^{\mu\nu} = 0$. In the ideal hydrodynamics, the energy-momentum tensor becomes $T^{\mu\nu} = (e + P)u^\mu u^\nu - Pg^{\mu\nu}$, where e is the energy density, P is the pressure, and u^μ is the four fluid velocity. When there are conserved quantities such as the baryon number or the number of chemically frozen hadrons, one needs to solve the continuity equations $\partial_\mu n_i^\mu = 0$ together with the hydrodynamic equations. In order to close the system of partial differential equations, the equation of state (EoS) $P(e, n_i)$ is needed. It is the EoS that governs the dynamics of the system in the ideal hydrodynamics. The naive applicability conditions of ideal hydrodynamics are that the mean free path among the particles is much smaller than the typical size of the system and that the system keeps local thermal equilibrium during expansion. From these conditions, one cannot use hydrodynamics for initial collisions, final free streaming and high p_T ($\gtrsim 2$ GeV/ c) particles. The quantitative criteria are more complicated in general since these come from dynamical aspects of the space-time evolution.

One usually assumes the initial hydrodynamic fields at initial (or equilibrated) time around 1 fm/ c . One needs an interface between the pre-thermalisation stage and the hydrodynamic stage at the initial time. On the other hand, the system eventually breaks up and the assumption of the thermalisation is no longer valid at the later stage. This means a prescription of freezeout is needed in the hydrodynamic model when one evaluates the particle spectra to be observed by the detectors. Then one needs another interface between the hydrodynamic stage and the free streaming stage. In what follows, we discuss particularly equation of state, initial condition and freezeout prescription used in the literature.

1.2.1. Equation of State The main ingredient of the hydrodynamic model is the equation of state (EoS) for thermalised matter produced in heavy ion collisions. Ideally, one uses the EoS taken from the first principle calculations of QCD, namely, lattice QCD simulations [16]. More practically, one can use the resonance gas model for the hadron phase and the massless free parton gas for the QGP phase. By matching these two EoS's at the critical temperature, one obtains the first order phase transition model with a latent heat ~ 1 GeV/fm³. In the mixed phase in this model, the sound velocity $c_s^2 = \frac{\partial P}{\partial e}$ is vanishing. Recent lattice QCD simulations tell us that the phase transition seems to be crossover in vanishing baryonic chemical potential. Although the discontinuity of the thermodynamic variables do not exist in the crossover phase transition, it should be emphasized that the energy density and the entropy density increase more rapidly than the pressure in the vicinity of the phase transition region $\Delta T \sim 0.1T_c$. This also leads to very small sound velocity near the phase transition region. Therefore it is very hard to find flow observables which distinguish the crossover phase transition with a rapid

change of the thermodynamic variables from the first order phase transition.

The statistical model and the blast wave model tell us that chemical freezeout temperature T^{ch} is larger than thermal freezeout temperature T^{th} at the RHIC energies (see, e.g., discussions in Ref. [17]). Chemical freezeout temperature obtained from the statistical model analysis is very close to the (pseudo)critical temperature of the QCD phase transition. This means that the hadron phase is almost chemically frozen due to strong expansion. For chemically frozen hadronic gas, one introduces chemical potential for each hadron [18]. This modifies the chemical composition in the hadron phase compared with the chemical equilibrium hadronic gas and, consequently, changes the space-time evolution of temperature field [19].

1.2.2. Initial Condition Once initial conditions are assigned, one can numerically simulate the space-time evolution of thermalised matter which is governed by hydrodynamic equations. Usually, initial conditions are parametrised based on some physical assumptions. Transverse profile of the energy/entropy density is assumed to be proportional to the local number of participants ρ_{part} , the local number of binary collisions ρ_{coll} or linear combination of them. Initial transverse flow is usually taken to be vanishing. In either full three dimensional (3D) hydrodynamic simulations or hydrodynamic simulations of longitudinal expansion with cylindrically symmetric geometry, one needs to parametrise also longitudinal profile of initial conditions for energy density, baryon density and four fluid velocity. The initial longitudinal shape is chosen so as to reproduce the final (pseudo)rapidity distribution of hadrons. Unfortunately, the shape is not uniquely determined. Two completely different initial conditions can end up almost similar rapidity distribution. See, e.g., Ref. [20].

On the other hand, one can introduce model calculations to obtain the initial condition of hydrodynamic simulations. Event generators can be used to obtain the energy density distribution at the initial time. Recently, the SPHeRIO group employs an event generator NeXus and takes an initial condition from this model in the event-by-event basis [21]. The resultant energy density distribution in the transverse plane has highly bumpy structures [21, 22]. Smooth initial conditions used in the conventional hydrodynamic simulations are no longer expected in one event. Another important example which is relevant at very high collision energies is an initial condition taken from the Colour Glass Condensate picture [23]. This will be discussed in details in Sec. 2.

1.2.3. Freezeout Conventional prescription to obtain the invariant momentum spectra from the hydrodynamic simulations is to employ the so-called Cooper-Frye formula [24]

$$E \frac{dN_i}{d^3p} = \frac{d_i}{(2\pi)^3} \int_{\Sigma(x)} \frac{p^\mu d\sigma_\mu(x)}{\exp[(p^\nu u_\nu(x) - \mu_i(x))/T(x)] \pm 1} \quad (3)$$

where $p^\mu = (E, \mathbf{p})$ and d_i are, respectively, a four momentum and the degree of freedom of a particle under consideration. Integral is performed on the freezeout hypersurface Σ . Here $d\sigma$ is an element of freezeout hypersurface on Σ . One usually assumes

$\Sigma = \Sigma(T = T^{\text{th}}$ or $e = e^{\text{th}}$), where T^{th} (e^{th}) is thermal freezeout temperature (energy density). T^{th} or e^{th} is an adjustable parameter for reproduction of the slope of p_T spectrum. Information on the hydrodynamic simulations is taken through $d\sigma$, u^μ , T and μ_i at a space-time point x . Chemical potential for each hadron μ_i is not vanishing in general even in vanishing baryon density due to $T^{\text{ch}} > T^{\text{th}}$. Although the chemical potential is important to reproduce the particle ratios as well as the shape of the particle spectra, this is often neglected for simplicity in the literature.

The physical picture described by the Cooper-Frye formula is sometimes called “sudden freezeout” since the mean free path λ is suddenly changed from zero to infinity through a thin freezeout hypersurface. Instead of using this, one can use a hadronic cascade model to describe the space-time evolution of hadrons [25, 26]. The mean free path among hadrons is finite and depends on hadronic species. Hence, one can describe a continuous freezeout picture through hadronic transport models. Note that continuous particle emission can be considered within the hydrodynamics [27]. Adoption of hadronic transport models after hydrodynamic evolution of the QGP liquid could refine the dynamical modeling of relativistic heavy ion collisions. However, it is not so easy to connect them in a systematic and proper way. One has to use Eq. (3) again for the boundary between the QGP liquid and the hadron gas. However, Eq. (3) describes not only out-going particles $p^\mu d\sigma_\mu > 0$ but also in-coming particles $p^\mu d\sigma_\mu < 0$. If one uses hydrodynamic simulations as inputs for hadronic cascade models, one must discard the in-coming particles, which violates the energy-momentum conservation. In order to remedy this problem, one need to solve hydrodynamic equations *together with* the appropriate kinetic equations [28].

1.3. Hydrodynamic Results for v_2

We show comparison of the hydrodynamic results with the experimental data for $v_2(p_T)$, $v_2(\eta)$ at the RHIC energy and the excitation function of v_2 .

1.3.1. $v_2(p_T)$ With a help of assuming the Bjorken flow [29] for the longitudinal direction, one can solve the hydrodynamic equations only in the transverse plane at midrapidity. Systematic studies based on this (2+1)-dimensional hydrodynamic model are performed in Ref. [2]. For the EoS, complete chemical equilibrium is assumed for both the QGP phase and the hadron phase. p_T dependences of v_2 for pions and protons from this model [8] are compared with the STAR data [30] in Fig. 2 (left). By employing the EoS with phase transition, the hydrodynamic model correctly reproduces $v_2(p_T)$ and its mass-splitting behavior below $p_T = 1$ GeV/ c . On the other hand, $v_2(p_T)$ for (anti)protons from the resonance gas model does not agree with the data. Although the reason for the difference of the result between these two EoS models is not so clear, the experimental data favors the QGP EoS. Due to the assumption of chemical equilibrium in the hadron phase, this model does not reproduce particle ratio and spectra simultaneously. It is of importance to study whether the agreement with

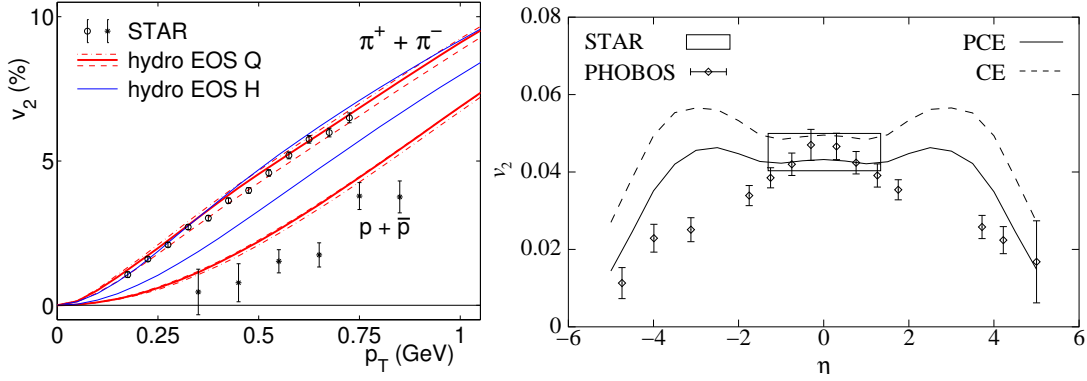


Figure 2. (left) Transverse momentum dependence of v_2 for pions and (anti)protons [8] are compared with the STAR data [30] in minimum bias Au+Au collisions at $\sqrt{s_{NN}} = 130$ GeV. EoS Q stands for the equation of state with first order phase transition between the massless free parton gas and the resonance gas. On the other hand, EoS H stands for the equation of state for the resonance gas. (right) v_2 for charged hadrons as a function of pseudorapidity η in Au+Au collisions at $\sqrt{s_{NN}} = 130$ GeV [1, 32]. PCE means the EoS of partial chemical equilibrium, whereas CE means the EoS of chemical equilibrium. Figure is taken from Ref. [19].

the experimental data still holds even when the assumption of chemical equilibrium in the hadron phase is abandoned [19].

1.3.2. $v_2(\eta)$ One needs a full 3D hydrodynamic simulation to obtain the rapidity dependence of v_2 since either cylindrical symmetry or Bjorken flow [29] keeps us from obtaining this quantity. First analysis of $v_2(\eta)$ at RHIC based on the full 3D hydrodynamic model is performed in Ref. [31]. After that, the effect of early chemical freezeout on the elliptic flow is also investigated [19]. Figure 2 (right) shows $v_2(\eta)$ for charged hadrons in Au+Au collisions at $\sqrt{s_{NN}} = 130$ GeV [1, 32]. Here the initial condition for the energy density is so chosen as to reproduce the pseudorapidity distribution of charged hadrons. Hydrodynamic results are consistent with the experimental data only near the midrapidity while hydrodynamics overpredicts the data in the forward/backward rapidity regions. Multiplicity is not so large in the forward/backward rapidity regions, so equilibration of the system tends to be spoiled.

1.3.3. Excitation function Figure 3 shows the excitation function of v_2 compiled by the STAR Collaboration [33]. Hydrodynamic results presented in this figure are based on the same model discussed in Sec. 1.3.1. Data points continuously increase with the unit rapidity density at the AGS, SPS and RHIC energies. However, the hydrodynamic response is almost flat or slightly decreases with the multiplicity. The data points seem to reach the “hydrodynamic limit” for the first time at the RHIC energy. It will be interesting to see the same plots including the upcoming LHC results: If the system produced at LHC obeys the hydrodynamic picture, this experimental “curve” will bend at $(1/S)dN/dy \sim 25-30$.

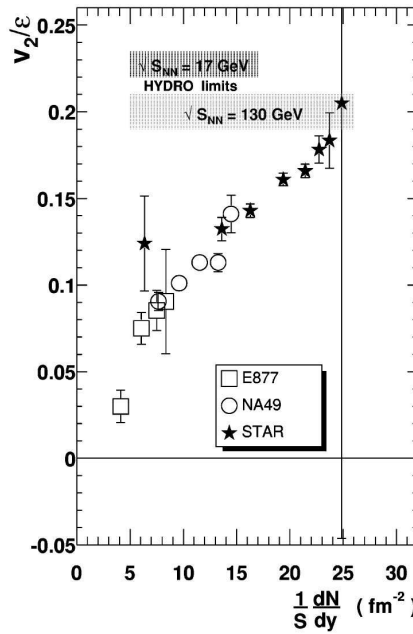


Figure 3. Excitation function of v_2/ε . Figure taken from Ref. [33].

The deviation between the hydrodynamic results and the data plots below $(1/S)dN/dy = 25$ reminds us the pseudorapidity dependence of elliptic flow in Fig. 2 (right). The deviation might come from a common origin [34]: the small multiplicity both in forward rapidity region at the RHIC energy and at midrapidity at the lower collision energies could cause the partial thermalisation. In the low density limit, v_2 is actually proportional to the number density [35]. The shape of $v_2(\eta)$ data in forward rapidity region looks similar to that of the pseudorapidity distributions [36]. Similarly, data plots of excitation function increase almost linearly with the particle density. These results suggest that thermalisation is not achieved completely in forward rapidity region at the RHIC energy and at midrapidity at the SPS energies.

Figure 4 shows the excitation function based on the hydro+cascade model [26] with Bjorken longitudinal flow [29]. In the hadron phase, a hadronic event generator RQMD is employed in these calculations. Contrary to the conventional hydrodynamic models, freezeout processes are automatically described by this model without any adjustable parameters. The excitation function in the case of the latent heat $\sim 0.8 \text{ GeV/fm}^3$ linearly increases with the multiplicity, which is consistent with the experimental data. It should be noted that $v_2(p_T)$, its mass dependences and particle spectra/ratio at midrapidity are also reproduced by this hybrid model [26].

1.4. Summary and Outlook

The most successful approach based on the hydrodynamic model to elliptic flow in relativistic heavy ion collisions is the hybrid one in which the QGP phase is described by the ideal hydrodynamics while the hadron phase is described by a hadronic cascade.

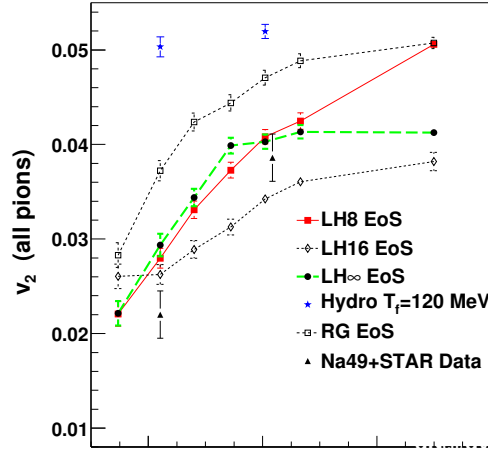


Figure 4. Excitation function from the hydro+cascade model. Figure taken from Ref. [26].

The Bjorken scaling solution [29] is assumed in the current hydro+cascade model. This means that current hybrid models are available only near midrapidity. Therefore it is desired to develop a model in which a full 3D hydrodynamic simulation is combined with a hadronic cascade model. From agreement of excitation function between the hybrid model and the experimental data at midrapidity, the 3D hybrid model is expected to reproduce the pseudorapidity dependence of elliptic flow. It should be emphasised again that the hybrid model has its own problem on the violation of energy momentum conservations between the QGP liquid and the hadron gas. A simulation which incorporates a proper treatment at the boundary between the QGP phase and the hadron phase is now an open problem.

2. Hydrodynamic Model with a CGC Initial Condition

2.1. Toward a Unified Description of Relativistic Heavy Ion Collisions

As already discussed in the previous section, one of the important findings at RHIC is that the hydrodynamic approach to the description of elliptic flow works remarkably well when early thermalisation time and the QGP EoS are assumed [7, 8]. Hydrodynamics should work only in the situation that the mean free path $\lambda = 1/\sigma\rho$ is much smaller than the typical size of the system L . This suggests that the particle density ρ becomes very large at RHIC.

In addition to this, there are many important findings in heavy ion collisions at the RHIC energy. One of them is jet quenching [37], i.e., suppression of high p_T hadrons in the single particle spectra and disappearance of away-side peak in the di-hadron spectra. These phenomena are not found in dAu collisions [38, 39, 40, 41]: the yield of high p_T hadrons roughly scales with the number of binary collisions N_{coll} and the away-side peak

appears in the di-hadron spectra. So one can conclude that high p_T partons produced in the initial hard scattering interact with the highly *dense* medium in the final state and that these partons lose their energies during traversing medium.

So the current RHIC data strongly suggest that the parton density created in heavy ion collisions at RHIC is dense enough to cause both large elliptic flow of bulk matter and large suppression of high- p_T hadrons. What is an origin of this dense matter at RHIC? The bulk particle production in high energy hadronic/nuclear collisions is dominated by the small x modes in the nuclear wave function, where x is a momentum fraction of the incident particles. Hence, an origin of the large density could be traced to the initial parton density at small x inside the ultra-relativistic nuclei before collisions. It is well known that the gluon density increases rapidly with decreasing x until gluons begin to overlap in the phase space where nonlinear interaction becomes important [42]. These gluons eventually form another type of extremely dense matter, the Colour Glass Condensate (CGC) [43]. This phenomenon is characterised by a “saturation scale” Q_s^2 which is identified with the gluon rapidity density per unit transverse area. When Q_s is sufficiently larger than the typical hadronic scale ($Q_s \gg \Lambda_{\text{QCD}}$), the strong coupling constant becomes weak ($\alpha_s(Q_s) \ll 1$). Moreover, the gluon occupation number in the wave function becomes huge, $\sim 1/\alpha_s(Q_s) \gg 1$. Therefore the CGC can be studied by a weak coupling classical method also known as McLerran-Venugopalan (MV) model [44]. The calculations based on the CGC picture have been compared to various RHIC data. Remarkably, the CGC results on the global observables, e.g., the centrality, rapidity and energy dependences of charged hadron multiplicities agree with the RHIC data under the assumption of parton-hadron duality [45].

In relativistic heavy ion collisions, the CGC could be a seed of the QGP [46]. So hydrodynamic initial conditions can be calculated from the two CGC collisions. One needs a non-equilibrium model which describes equilibration from the produced gluon distribution to a local thermal distribution. This is, however, beyond the present work. In this work, the rapidity, transverse position and centrality dependences of the number of produced gluons are identified with the hydrodynamic initial condition of a thermalised QGP.

Some of the problems which are inherent in a particular approach can be removed. For instance, one conventionally parametrises initial conditions in the hydrodynamic simulations shortly after a collision of two nuclei by hand. Therefore it is desired to take an initial condition which is obtained by a reliable theory. On the other hand, most of the calculations based on the CGC do not include final state interactions. According to estimation of initial parton productions from a classical lattice Yang-Mills simulation based on the CGC [47, 48], the transverse energy per particle is roughly $E_T/N \sim 1.5$ GeV, while the experimental data yields $E_T/N \sim 0.6$ GeV [49]. Moreover, elliptic flow from a classical Yang-Mills simulation is inconsistent with RHIC data [50]. Those discrepancies, which are mainly due to the lack of collective effects, will be removed by introducing further time evolution through, e.g., hydrodynamics. For the calculation of parton energy loss, one needs time evolution of parton density. Bjorken expansion [29]

is assumed for the evolution of parton density in almost all work except Refs. [51, 52].

We have already developed a unified model (CGC+Hydro+Jet model) in which hydrodynamic evolution, CGC initial conditions, and the production and propagation of high p_T partons are combined [23]. Only the soft sector, i.e., the production of gluons in CGC collisions and the hydrodynamic afterburner for the CGC initial condition is discussed in this paper. For further details of the model and the results for high p_T regions such as centrality dependences of the nuclear modification factors and the azimuthal correlation functions, see Ref. [23].

2.2. Gluon Production from a CGC picture

We employ the k_T factorisation formula for the production of gluons from CGC collisions along the line of work by Kharzeev, Levin and Nardi (KLN) [45]. The number of produced gluons in the k_T -factorisation formula is given by [42, 53, 54, 55]

$$\frac{dN_g}{d^2x_\perp dy} = \frac{4\pi^2 N_c}{N_c^2 - 1} \int \frac{d^2p_T}{p_T^2} \int d^2k_T \alpha_s(Q^2) \times \phi_A(x_1, k_T^2; \mathbf{x}_\perp) \phi_B(x_2, (p_T - k_T)^2; \mathbf{x}_\perp), \quad (4)$$

where $x_{1,2} = p_T \exp(\pm y)/\sqrt{s}$, and y and p_T are a rapidity and a transverse momentum of a produced gluon. Running coupling constant α_s is evaluated at the scale $Q^2 = \max(k_T^2, (p_T - k_T)^2)$. The unintegrated gluon distribution ϕ is related to the gluon density of a nucleus by

$$xG_A(x, Q^2) = \int^{Q^2} d^2k_T d^2x_\perp \phi_A(x, k_T^2; \mathbf{x}_\perp). \quad (5)$$

Motivated by the KLN approach, we use a simplified assumption about the unintegrated gluon distribution function:

$$\phi_A(x, k_T^2; \mathbf{x}_\perp) = \begin{cases} \frac{\kappa C_F}{2\pi^3 \alpha_s(Q_s^2)} \frac{Q_s^2}{Q_s^2 + \Lambda^2}, & k_T \leq Q_s, \\ \frac{\kappa C_F}{2\pi^3 \alpha_s(Q_s^2)} \frac{Q_s^2}{k_T^2 + \Lambda^2}, & k_T > Q_s, \end{cases} \quad (6)$$

where $C_F = (N_c^2 - 1)/(2N_c)$. We introduce a small regulator $\Lambda = 0.2$ GeV/ c in order to have a smooth distribution in the forward rapidity region $|y| > 4.5$ at RHIC. Other regions are not affected by introducing a small regulator. The above distribution depends on the transverse coordinate \mathbf{x}_\perp through Q_s^2 . Saturation momentum of a nucleus A in $A + B$ collisions is obtained by solving the following implicit equation with respect to Q_s at fixed x and \mathbf{x}_\perp

$$Q_s^2(x, \mathbf{x}_\perp) = \frac{2\pi^2}{C_F} \alpha_s(Q_s^2) xG(x, Q_s^2) \rho_{\text{part}}^A(\mathbf{x}_\perp), \quad (7)$$

where

$$\rho_{\text{part}}^A(\mathbf{x}_\perp) = T_A(\mathbf{x}_\perp) \left\{ 1 - [1 - \sigma_{NN}^{\text{in}} T_B(\mathbf{x}_\perp)/B]^B \right\}. \quad (8)$$

The number of participants is given by

$$N_{\text{part}} = \int d^2x_\perp (\rho_{\text{part}}^A(\mathbf{x}_\perp) + \rho_{\text{part}}^B(\mathbf{x}_\perp)). \quad (9)$$

We take a simple perturbative form for the gluon distribution in a nucleon

$$xG(x, Q^2) = K \ln \left(\frac{Q^2 + \Lambda^2}{\Lambda_{\text{QCD}}^2} \right) x^{-\lambda} (1-x)^n \quad (10)$$

where $\Lambda = \Lambda_{\text{QCD}} = 0.2$ GeV. K is used to control saturation scale in Eq. (7) [56]. We choose $K = 0.7$ for $\lambda = 0.2$ so that the average saturation momentum in the transverse plane yields $\langle Q_s^2(x = 0.01) \rangle \sim 2.0$ GeV²/c² in Au+Au collisions at impact parameter $b = 0$ at RHIC. Similar to the KLN approach, $x^{-\lambda}$ dependence of the saturation scale is motivated by the Golec-Biernat–Wüsthoff model [57]. The factor $(1-x)^n$ shows that gluon density becomes small at $x \rightarrow 1$. n usually depends on the scale Q^2 . Here we take $n = 4$ as in the KLN approach [45].

We obtain the rapidity distribution for produced gluons at each transverse point \mathbf{x}_\perp by performing the integral of Eq. (4) numerically. The transverse energy distribution dE_T/dy is also obtained by weighting the transverse momentum of gluons p_T in the integration with respect to p_T in Eq. (4). We cut off the integral range of p_T in Eq. (4) since only the low p_T partons are assumed to reach the local thermal equilibrium. We set the cut-off momentum as $p_{T,\text{cut}} = 3$ GeV/c which corresponds roughly to the maximum saturation scale at $x = 0.01$ at the origin $\mathbf{x}_\perp = \mathbf{0}$ in central Au+Au collisions at RHIC.

In order to obtain initial conditions for hydrodynamics, one needs a non-equilibrium description for the collisions of heavy nuclei. Leaving this problem for the future work, we assume that the system of gluons initially produced from the CGC reaches a kinematically and chemically equilibrated state at a short time scale.

There are two ways to provide initial conditions from the CGC, i.e., matching of number density (IC- n) and matching of energy density (IC- e). Here, we employ the former prescription, i.e., IC- n . For the result from IC- e , see Ref. [23]. Assuming Bjorken's ansatz $y = \eta_s$ [29] where η_s is the space-time rapidity $\eta_s = (1/2) \ln(x^+/x^-)$, we obtain the number density for gluons at a space-time point $(\tau_0, \mathbf{x}_\perp, \eta_s) \equiv (\tau_0, \vec{x})$ from Eq. (4)

$$n_g(\tau_0, \vec{x}) = \frac{dN_g}{\tau_0 d\eta_s d^2x_\perp}. \quad (11)$$

Number density n for the massless free parton system can be written:

$$n = \left(\frac{3}{4} d_q + d_g \right) \frac{\zeta(3)}{\pi^2} T^3, \quad (12)$$

where $d_q = 2N_c N_s N_f = 36$, $d_g = 2(N_c^2 - 1) = 16$ and $\zeta(3) = 1.20206$. Thus, we obtain the initial temperature field in the three-dimensional (3D) space from the number density (IC- n):

$$T(\tau_0, \vec{x}) = \left\{ \frac{\pi^2 n(\tau_0, \vec{x})}{43\zeta(3)} \right\}^{1/3}. \quad (13)$$

When the temperature at (τ_0, \vec{x}) is below the critical temperature $T_c = 170$ MeV, the all thermodynamic variables in the cell are set to zero.

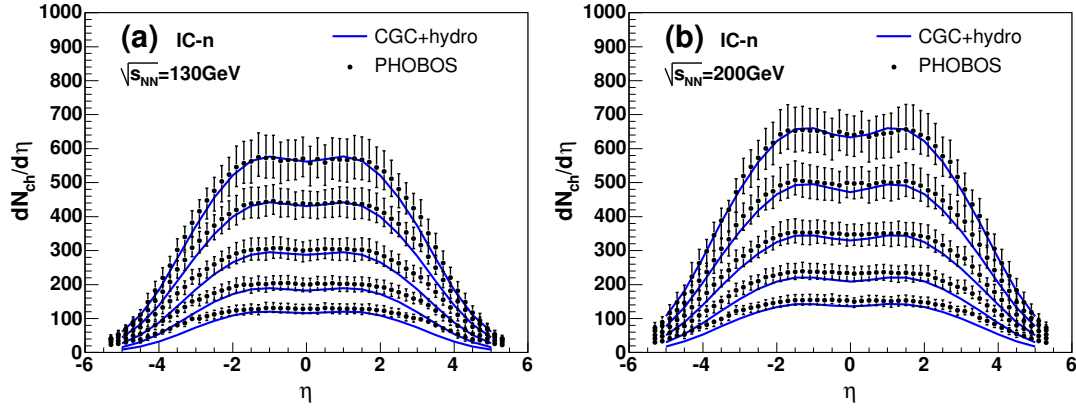


Figure 5. Pseudorapidity distributions of charged hadrons in Au + Au collisions at $\sqrt{s_{NN}} =$ (a) 130 and (b) 200 GeV are compared to the PHOBOS data [58]. Figure taken from Ref. [23]

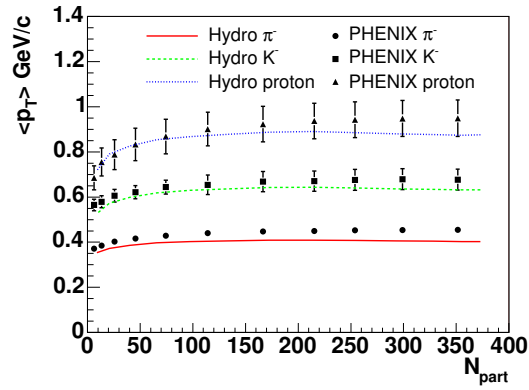


Figure 6. Mean transverse momenta for pions, kaons and protons as a function of N_{part} [59]. Here contribution only from hydrodynamic components is taken into account. $T^{\text{th}} = 100$ MeV is used for all centralities. Figure taken from Ref. [23]

2.3. Results

In Fig. 5, pseudorapidity distributions of charged hadrons in Au + Au collisions at both $\sqrt{s_{NN}} = 130$ and 200 GeV are compared with the PHOBOS data [58]. Impact parameters in each panel are, from top to bottom, 2.4, 4.5, 6.3, 7.9, and 9.1 fm (2.5, 4.4, 6.4, 7.9, and 9.1 fm) for $\sqrt{s_{NN}} = 200$ (130) GeV. These impact parameters are evaluated from the average number of participants at each centrality estimated by PHOBOS [58]. It should be also emphasized that it is not easy to parametrize such initial conditions which reproduce the data with the same quality as the CGC initial conditions presented here.

Mean transverse momenta $\langle p_T \rangle$ for pions, kaons and protons as a function of N_{part} are compared with the PHENIX data [59] in Fig. 6. Although our results are slightly smaller than the data in central and semicentral regions, the overall trend is consistent

with the data. For pions, the semihard spectrum starts to be comparable with the soft spectrum around $p_T = 1.5\text{-}2.0$ GeV/ c . We reproduce the p_T spectra for pions by including contribution from quenched jets. So the deviation for pions can be filled by the semihard spectrum. While semihard components for kaons and protons are very small in low and intermediate p_T regions. A little more radial flow is needed to gain the mean transverse momentum in central collisions.

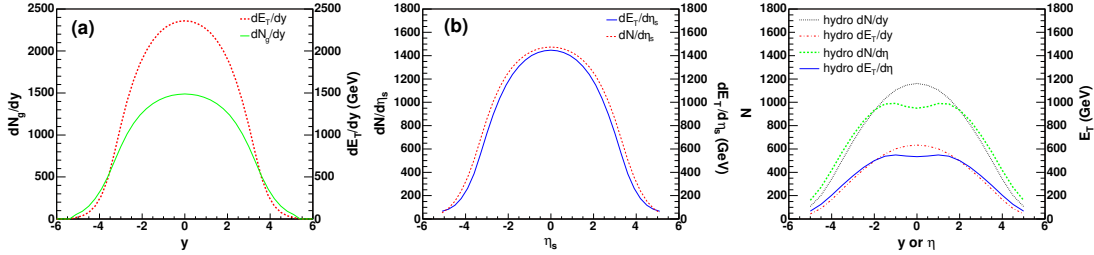


Figure 7. (Pseudo)rapidity distribution of (a) gluons produced from CGC collisions, (b) partons at initial time, and (c) final total hadrons in Au + Au collisions at $\sqrt{s_{NN}} = 200$ GeV.

Both the KLN approach and the hydrodynamic model with a CGC initial condition reproduce the centrality and rapidity dependences of particle distributions. Then, what is the role of hydrodynamic evolution in comparison with the KLN approach? The main difference between these two approaches is whether final state interactions are taken into account. The initial transverse energy per particle is estimated to be $E_T/N_g \sim 1.6$ GeV at $y = 0$. It becomes $E_T/N_g = 1.0$ GeV after assuming a thermal state. The effect of the hydrodynamic afterburner is to reduce the transverse energy per particle due to pdV work. We find that $(dE_T/dy)/(dN/dy)|_{y=0} = 0.54$ GeV and $(dE_T/d\eta)/(dN/d\eta)|_{\eta=0} = 0.56$ GeV.

2.4. Summary and Outlook

Our approach is a first step toward a unified dynamical modeling of relativistic heavy ion collisions.

The main goal has been developing a consistent dynamical framework for the space-time evolution of both bulk matter and hard jets. In order to accomplish this, much remains are to be done.

- More sophisticated wave function should be used to calculate the production of initial gluons. At midrapidity, results from the classical Yang-Mills equation can be used. In forward rapidity region at the RHIC energy or even at midrapidity at the LHC energy, one needs a quantum evolution.
- As discussed in the Sec. 1, the hadron phase should be described by a hadronic transport model. This will improve v_2 in forward rapidity regions in the hydrodynamic result.

- EoS from the recent lattice QCD simulations should be used in the hydrodynamic simulations.
- Chemical non-equilibrium process will be taken into account by solving the rate equation for the number of quarks and gluons together with the hydrodynamic equations [60]. The amount of energy loss of partons depends on a species of both probe parton and medium parton. So the correct chemical composition in the QGP phase will lead to reproduction of nuclear modification factors without any free parameters.

Acknowledgments

One of the authors (T.H.) would like to thank the organizers of this workshop for invitation. The work by T.H. was supported by RIKEN.

Reference

- [1] Ackermann K H *et al* (STAR Collaboration) 2001 *Phys. Rev. Lett.* **86** 402
- [2] Kolb P F, Huovinen P, Heinz U and Heiselberg H 2001 *Phys. Lett. B* **500** 232
Huovinen P, Kolb P F, Heinz U W, Ruuskanen P V and Voloshin S A 2001 *Phys. Lett. B* **503** 58
Kolb P F, Heinz U W, Huovinen P, Eskola K J and Tuominen K 2001 *Nucl. Phys.* **A696** 197
- [3] Alt C *et al* (NA49 Collaboration) 2003 *Phys. Rev. C* **68** 034903
Agakichiev G *et al* (CERES/NA45 Collaboration) 2004 *Phys. Rev. Lett.* **92** 032301
- [4] Shuryak E 2004 *J. Phys. G: Nucl. Part. Phys.* **30** S1221
Teaney D 2003 *Phys. Rev. C* **68** 034913
- [5] Bleicher M and Stocker H 2002 *Phys. Lett. B* **526** 309
- [6] Retière F 2004 *J. Phys. G: Nucl. Part. Phys.* **30** S827
- [7] Huovinen P 2003 *Preprint* nucl-th/0305064
- [8] Kolb P F and Heinz U 2003 *Preprint* nucl-th/0305084
- [9] Ollitrault J Y 1992 *Phys. Rev. D* **46** 229
Ollitrault J Y 1998 *Nucl. Phys. A* **638** 195
- [10] Poskanzer A M and Voloshin S A 1998 *Phys. Rev. C* **58** 1671
- [11] Kolb P 2003 *Phys. Rev. C* **68** 031902
- [12] Adams J *et al* (STAR Collaboration) 2004 *Phys. Rev. Lett.* **92** 062301
- [13] Kolb P F, Sollfrank J and Heinz U W 2000 *Phys. Rev. C* **62** 054909
- [14] Molnar D and Huovinen P 2004 *Preprint* nucl-th/0404065
- [15] Muronga A 2004 *Phys. Rev. C* **69** 034903
Muronga A and Rischke D H 2004 *preprint* nucl-th/0407114
- [16] Karsch F 2002 *Lect. Notes Phys.* **583** 209
- [17] Shuryak E V 1999 *Nucl. Phys. A* **661** 119
Heinz U 1999 *Nucl. Phys. A* **661** 140
- [18] Bebie H, Gerber P, Goity J L and Leutwyler H 1992 *Nucl. Phys. B* **378** 95
- [19] Hirano T and Tsuda K 2002 *Phys. Rev. C* **66** 054905
- [20] Huovinen P, Ruuskanen P V and Sollfrank J 1999 *Nucl. Phys. A* **650** 227
- [21] Osada T, Aguiar C E, Hama Y and Kodama T 2001 *Preprint* nucl-th/0102011
Hama Y, Kodama T and Socolowski Jr O 2004 *hep-ph/0407264*
- [22] Gyulassy M, Rischke D H and Zhang B 1997 *Nucl. Phys. A* **613** 397
- [23] Hirano T and Nara Y 2004 *Nucl. Phys. A* (in press)
- [24] Cooper F and Frye G 1974 *Phys. Rev. D* **10** 186

- [25] Bass S A and Dumitru A 2000 *Phys. Rev. C* **61** 064909
- [26] Teaney D, Lauret J and Shuryak E V 2001 *Preprint* nucl-th/0110037
- [27] Grassi F, Hama Y and Kodama T 1995 *Phys. Lett. B* **355** 9
Socolowski O J, Grassi F, Hama Y and Kodama T 2004 *Preprint* hep-ph/0405181
- [28] Bugaev K A 2003 *Phys. Rev. Lett.* **90** 252301
Bugaev K A 2004 *Preprint* nucl-th/0401060
- [29] Bjorken J D 1983 *Phys. Rev. D* **27** 140
- [30] Adler C *et al* (STAR Collaboration) 2001 *Phys. Rev. Lett.* **87** 182301
- [31] Hirano T 2001 *Phys. Rev. C* **65** 011901
- [32] Back B B *et al* (PHOBOS Collaboration) 2002 *Phys. Rev. Lett.* **89** 222301
- [33] Adler C *et al* (STAR Collaboration) 2002 *Phys. Rev. C* **66** 034904
- [34] Heinz U and Kolb P 2004 *J. Phys. G: Nucl. Part. Phys.* **30** S1229
- [35] Heiselberg H and Levy A M 1999 *Phys. Rev. C* **59** 2716
- [36] Steinberg P A 2002 *Nucl. Phys. A* **698** 314c
- [37] Gyulassy M, Vitev I, Wang X N and Zhang B W 2003 *Preprint* nucl-th/0302077
Kovner A and Wiedemann U A 2003 *Preprint* hep-ph/0304151
- [38] Back B B *et al* (PHOBOS Collaboration) 2003 *Phys. Rev. Lett.* **91** 072302
- [39] Adler S S *et al* (PHENIX Collaboration) 2003 *Phys. Rev. Lett.* **91** 072303
- [40] Adams J *et al* (STAR Collaboration) 2003 *Phys. Rev. Lett.* **91** 072304
- [41] Arsene I *et al* (BRAHMS Collaboration) 2003 *Phys. Rev. Lett.* **91** 072305
- [42] Gribov L V, Levin E M and Ryskin M G 1983 *Phys. Rept.* **100** 1
- [43] Iancu E and Venugopalan R 2003 *Preprint* hep-ph/0303204
- [44] McLerran L D and Venugopalan R 1994 *Phys. Rev. D* **49** 2233
McLerran L D and Venugopalan R 1994 *Phys. Rev. D* **49** 3352
McLerran L D and Venugopalan R 1994 *Phys. Rev. D* **50** 2225
- [45] Kharzeev D and Nardi M 2001 *Phys. Lett. B* **507** 121
Kharzeev D and Levin E 2001 *Phys. Lett. B* **523** 79
Kharzeev D, Levin E and Nardi M 2001 *Preprint* hep-ph/0111315
Kharzeev D, Levin E and Nardi M 2004 *Nucl. Phys. A* **730** 448
- [46] Gyulassy M and McLerran L 2004 *Preprint* nucl-th/0405013
- [47] Krasnitz A, Nara Y and Venugopalan R 2003 *Nucl. Phys. A* **727** 427
- [48] Lappi T 2003 *Phys. Rev. C* **67** 054903
- [49] Bazilevsky A *et al* (PHENIX Collaboration) 2003 *Nucl. Phys. A* **715** 486c
- [50] Krasnitz A, Nara Y and Venugopalan R 2003 *Phys. Lett. B* **554** 21
- [51] Gyulassy M, Vitev I, Wang X N and Huovinen P 2002 *Phys. Lett. B* **526** 301
- [52] Hirano T and Nara Y 2002 *Phys. Rev. C* **66** 041901
Hirano T and Nara Y 2003 *Phys. Rev. Lett.* **91** 082301
Hirano T and Nara Y 2003 *Phys. Rev. C* **68** 064902
Hirano T and Nara Y 2004 *Phys. Rev. C* **69** 034908
- [53] Gribov L V, Levin E M and Ryskin M G 1981 *Phys. Lett. B* **100** 173
- [54] Laenen E and Levin E 1994 *Ann. Rev. Nucl. Part. Sci.* **44** 199
- [55] Szczurek A 2003 *Acta Phys. Polon. B* **34** 3191
- [56] Baier R, Kovner A and Wiedemann U A 2003 *Phys. Rev. D* **68** 054009
- [57] Golec-Biernat K and Wusthoff M 1999 *Phys. Rev. D* **59** 014017
Golec-Biernat K and Wusthoff M 1999 *Phys. Rev. D* **60** 114023
- [58] Back B B *et al* 2003 *Phys. Rev. Lett.* **91** 052303
- [59] Adler S S *et al* (PHENIX Collaboration) 2003 *Preprint* nucl-ex/0307022
- [60] Biro T S, van Doorn E, Muller B, Thoma M H and Wang X N 1993 *Phys. Rev. C* **48** 1275
Srivastava D K, Mustafa M G and Muller B 1997 *Phys. Rev. C* **56** 1064
Elliott D M and Rischke D H 2000 *Nucl. Phys. A* **671** 583